Cell-selective knockout and 3D confocal image analysis reveals separate roles for Astrocyte- and Endothelial-derived CCL2 in neuroinflammation

[1]Debayon Paul, [1]Shujun Ge, [1]Yen Lemire, [2]Evan R. Jellison, [3]David R. Serwanski, [4]Nancy H. Ruddle, [1]Joel S. Pachter

[1]Blood–Brain Barrier Laboratory & [2]Department of Immunology, UCHC, [3]Department of Physiology and Neurobiology, UConn,
[4]School of Public Health, Yale University, CT, USA

ABSTRACT

Expression of chemokine CCL2 in central nervous system (CNS) drives neuroinflammation during experimental autoimmune encephalomyelitis (EAE), an animal model of Multiple Sclerosis (MS), and is also known to play a role in MS. As astrocytes and brain microvascular endothelial cells are known major CNS sources of CCL2, mice with targeted CCL2 gene knockout *(KO)* in astrocytes (*Astro KO*) or endothelial cells (*Endo KO*) were employed to evaluate their respective contributions to EAE pathogenesis following myelin oligodendrocyte glycoprotein peptide (MOG_{35-55}) immunization. High-resolution 3D immunofluorescence confocal microscopy and colloidal gold immuno-electron microscopy were employed to confirm sites of CCL2 expression. 3D confocal microscopy was further utilized to assess inflammatory responses along the CNS microvasculature. Cell-selective loss of CCL2 immunoreactivity was demonstrated in the respective *KO* mice. Compared to wild-type (*WT*) mice, *Astro KO* mice showed reduced EAE severity but similar onset, while *Endo KO* mice displayed near normal severity but a delayed onset. Neither of the *KO* mice showed deficits in T cell proliferation, or IL-17 and IFNγ production, following MOG_{35-55} exposure *in vitro*, or altered MOG-MHC class II tetramer binding. Using a novel, microvessel contour-based 3D confocal image visualization and analysis approach for immunostained spinal cord sections developed in our lab, we further showed *Astro KOs* lacked the CNS leukocyte entry and fragmented-pattern of Claudin-5 (CLN-5) immunostaining at the blood-brain barrier (BBB) seen during early EAE in *WT* mice, while *Endo KOs* uniquely displayed leukocytes stalled in the microvascular lumen. These results point to astrocyte and endothelial pools of CCL2 each regulating different stages of neuroinflammation in EAE, and carry implications for drug delivery in neuroinflammatory disease.

AIM

Determine the role(s) of Astrocytic and Endothelial-derived CCL2 in EAE progression, BBB damage, and leukocyte transendothelial migration (TEM).

METHODOLOGY

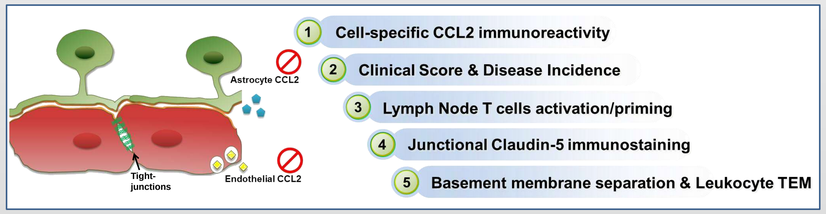

1. Cell-specific CCL2 immunoreactivity
2. Clinical Score & Disease Incidence
3. Lymph Node T cells activation/priming
4. Junctional Claudin-5 immunostaining
5. Basement membrane separation & Leukocyte TEM

RESULTS

CCL2 staining in *WT*, *Astro KO* and *Endo KO* mice during EAE

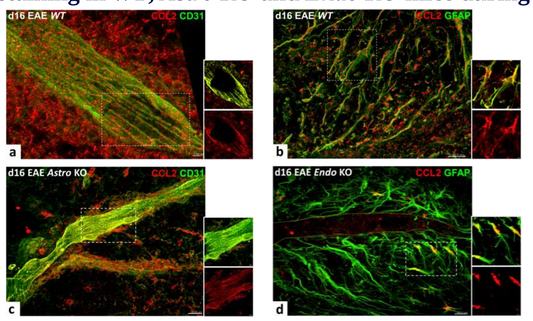

Fig 1. 3D reconstruction of 60µm confocal z-stacks from spinal cord sections revealing CCL2 expression, and CD31 or GFAP to delineate the endothelial cells and astrocytes respectively, in *WT*, *Astro KO* and *Endo KO* mice at d16 post-EAE. **(a)** *WT* mice show CCL2 along the $CD31^+$ microvascular endothelium, and perivascular space. **(b)** CCL2 staining is also associated with $GFAP^+$ astrocytes in *WT* mice. **(c)** *Astro KO* mice show venule-associated CCL2 staining, but lack staining in the parenchymal astrocytes. **(d)** In contrast, *Endo KO* mice are deficient in vessel-associated CCL2 staining, but maintain astrocyte staining. Insets demonstrate colocalization of CCL2 with CD31 or GFAP (yellow) in a single z-slice.

Astro KO and *Endo KO* mice display altered clinical EAE patterns

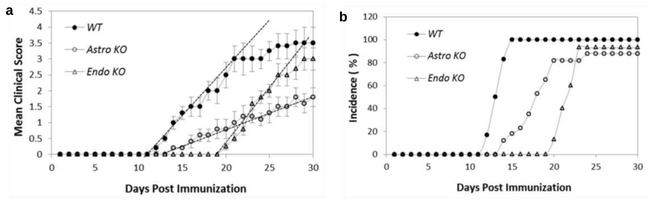

Fig 2. Clinical Score and Disease Incidence in *WT*, *Astro KO*, and *Endo KO* mice following EAE, scored daily for 30 days. **(a) Clinical Score**. *Astro KO* mice do not attain as severe disease as *WT*, while *Endo KO* mice approach *WT* disease severity but with a significantly delayed onset. **(b) Disease incidence**. All mice show a similar incidence of disease but, compared to *WT* mice, *Astro KO* mice show only a mild delay while *Endo KO* mice show a significant delay in disease onset.

Similar immune responses in LNC from *WT*, *Astro KO* and *Endo KO*

a

Summary of effects of *Astro KO* and *Endo KO* on LNC proliferation

Group	% Divided	Division index	Proliferation index	Expansion index	Replication index
WT	80.71 ± 9.01	1.60 ± 0.35	2.00 ± 0.37	4.53 ± 1.67	5.33 ± 1.89
Astro KO	83.98 ± 2.15	1.52 ± 0.37	2.02 ± 0.39	4.92 ± 1.88	5.67 ± 2.21
Endo KO	72.25 ±9.23	1.64 ± 0.19	2.32 ± 0.19	4.08 ± 0.45	5.52 ± 0.93

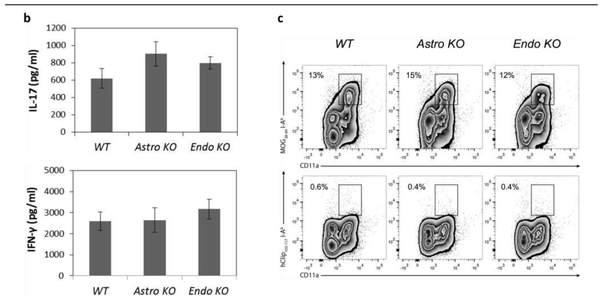

Fig 3. Lymph node cells (LNC) isolated from MOG_{35-55}-immunized mice on d12 were restimulated with MOG_{35-55} for 72 h in culture, following which the different immune responses were measured. **(a) T cell proliferation**. LNC were pulse-labeled with 2µM CFSE for 5 min at the beginning of culture and analyzed after 72 h by FACS, gating on CD3, CD4, CD11a. **(b) Cytokine production**. The concentrations of IL-17 and IFNγ were measured in supernatants of LNC after 72 h in culture. Data reflect Mean ± SEM. **(c) Binding of MOG_{38-49} MHC class II tetramer-PE**. Binding was determined after 72 h in culture, and $hCLIP_{103-117}$ tetramer-PE served as a control. Plots were gated on $CD4^+$ T lymphocytes. The frequency of MOG_{38-49} $I\text{-}A^b$ $tetramer^+$ $CD4^+$ T cells is similar among *WT*, *Astro KO*, and *Endo KO* groups, while $hCLIP_{103-117}$ $I\text{-}A^b$ tetramer does not bind cultured T cells.

Differential loss of CLN-5 in *WT*, *Astro KO* and *Endo KO* in EAE

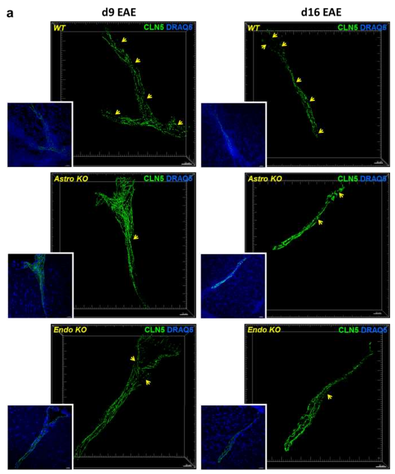

c

Group	CLN5 intensity/µm²		
	d9 EAE	vs.	d16 EAE
WT	15.04±1.09		7.13±0.74*
Astro KO	33.70±1.49		13.54±0.98*
Endo KO	21.83±2.32		16.86±0.91

CLN-5 density values expressed as Mean ± SEM; *$p \leq 0.0001$

Fig 4. **(a)** 3D perspective projection view of isosurface-rendered 60µm confocal z-stacks from *WT*, *Astro KO*, and *Endo KO* spinal cord sections at d9 and d16 EAE, stained for CLN-5 and nuclei/DRAQ5, showing the fragmented pattern of tight-junction (TJ) protein staining in EAE. Inserts highlight the close association of altered CLN-5 staining with dense perivascular cellularity representing infiltrating leukocytes. Arrows demark overt gaps in CLN-5 staining, suggesting TJ disruption. Notably, CLN-5 staining pattern during EAE appears most intact in *Astro KO*, least so in *WT*, and intermediate in *Endo KO* mice. **(b)** Quantification of CLN-5 staining intensity per unit surface area of the endothelium (CLN-5 density). CLN-5 density in naïve *WT* mice is shown as a reference for the normal state, wherein the CLN-5 staining is continuous. **(c)** Summary of CLN-5 changes. Data reflect Mean ± SEM. Scale = 20µm.

Differences in perivascular cellularity in *WT*, *Astro KO* and *Endo KO*

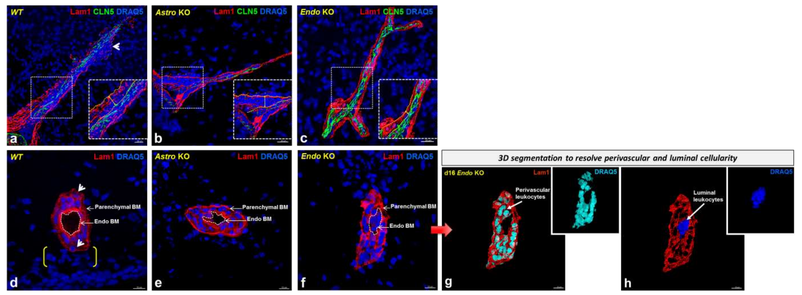

Fig 5. Isosurface-rendered 60µm z-stacks from spinal cryosections at d16 EAE, stained for basement membrane (BM) protein Laminin 1, CLN-5, and nuclei/DRAQ5 is shown. **(a, b, c)** Longitudinal sections highlight the extent of vessel-associated leukocytes. Insets represent enlarged view of areas in white boxes, while bidirectional arrows denote the 'perivascular space'. Scale = 20µm. **(d, e, f)** Cross-sections highlight the spatial distribution of leukocytes in the luminal or perivascular compartment. Scale = 10µm. **Perivascular Cellularity and BM integrity**: *WT* mice, show a dense accumulation of $DRAQ5^+$ perivascular cells (leukocytes), a few apparently penetrating the fragmented parenchymal BM. *Astro KO* mice, show similar perivascular cellularity, but visibly intact parenchymal BM, and lack parenchymal leukocytes. In *Endo KO* mice, the BM is seemingly intact, with minimal perivascular cellularity. **Luminal Cellularity**: In *WT* and *Astro KO* mice the vessel lumen appears empty; whereas, in *Endo KO* mice, cells are clearly present in the lumen. **(g-h) Red arrow** designates the same *Endo KO* image subject to *microvessel contour-based 3D segmentation* to further resolve luminal from perivascular nuclei.

3D distribution profiles of luminal and perivascular leukocytes

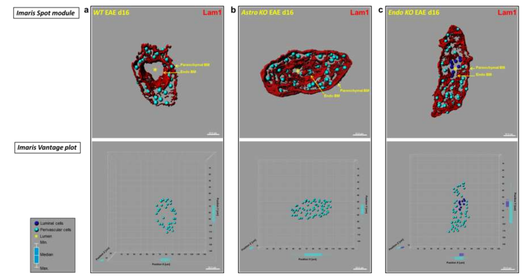

Fig 6. 3D reconstruction of confocal z-stacks from *WT*, *Astro KO*, and *Endo KO* spinal cord sections at d16 EAE, highlighting the BM with Laminin 1 staining. **Top row-** The luminal and perivascular compartments were optically isolated using *microvessel contour based 3D segmentation*, and the $DRAQ5^+$ cellularity were separated into luminal and perivascular nuclei. Using Imaris spot creation module, each of nuclei in the 3D dataset were rendered as "spot objects," designating its location. Scale = 10µm. **Bottom row-** Imaris vantage plots showing the 3D distribution of luminal and perivascular cells along the corresponding microvessels from top row. Scale = 20µm. **(a)** Representative *WT* vessel showing an empty lumen (*). **(b)** The lumen from *Astro KO* vessel also appears empty (*) but partially collapsed, possibly owing to accumulation of perivascular cells in absence of astrocyte-CCL2. **(c)** *Endo KO* vessel shows evidence of congregation of cells in the lumen, suggesting stalled leukocyte transmigration in absence of endothelial-CCL2. Box-and-whisker plots are shown indicating the max. and min. spread from the median, in µm, of luminal or perivascular nuclei along the x, y, and z-axes.

SUMMARY

Differential actions of astrocyte-derived and endothelial cell-derived CCL2

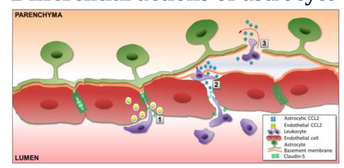

Fig 7. Schematic showing-

- ❑ Endothelial-derived CCL2 facilitates leukocyte migration across the endothelium **(1)**, a step post-adhesion.
- ❑ Astrocyte-derived CCL2 promotes both breakdown of endothelial tight-junctions **(2)**, and penetration of leukocytes across the parenchymal BM into the CNS parenchyma **(3)**.

REFERENCES

1. Paul D, Ge S1, Lemire Y, Jellison ER, Serwanski DR, Ruddle NH, Pachter JS. 2014. Cell-selective knockout and 3D confocal image analysis reveals separate roles for astrocyte-and endothelial-derived CCL2 in neuroinflammation. *J. Neuroinflammation*. 2014 Jan 21;11:10.
2. Paul, D., Cowan, A., Ge, S. and Pachter, J.S. 2013. Novel 3D analysis of claudin-5 reveals significant endothelial heterogeneity among CNS microvessels. *Microvascular Res*. 86:1-10.

ACKNOWLEDGEMENTS

This work was supported in part by grants 5RO1NSO61525-11 from the National Institutes of Health and RG4503A4/1 from the National Multiple Sclerosis Society to J.S.P.